»GREEN ICT @ FMD« – COMPETENCE CENTER FOR ECOLOGICALLY SUSTAINABLE ICT

Intelligent Sensor Systems for Energy-Efficient Monitoring of Production Processes

A Whitepaper by "HUB 1 –Sensor-Edge-Cloud"

Georg Roeder, Vincent Dreher, Martin Schellenberger (Fraunhofer IISB)

The work presented is part of the »Green ICT @ FMD« project, your competence center for ecologically sustainable information and communication technology. The project is established by the Research Fab Microelectronics Germany and funded by the German Federal Ministry of Research, Technology and Space.

Kompetenzzentrum »Green ICT @ FMD«

c/o Forschungsfabrik Mikroelektronik Deutschland FMD
Anna-Louisa-Karsch-Str. 2
10178 Berlin, Germany

Main contact
Georg Roeder, georg.roeder@iisb.fraunhofer.de

www.greenict.de
www.forschungsfabrik-mikroelektronik.de

Date of publication
19.12.2025

1. Summary

The demand for cost-efficient sensors in monitoring production processes has surged, driven by the need to optimize resource usage and enhance productivity. Industries are increasingly relying on sensors to gather real-time data for better decision-making, particularly in agriculture, water quality management, and various manufacturing processes. A frequent challenge observed in sensor technology is sensor drift, which can lead to inaccurate readings over time. This drift not only compromises data integrity but also necessitates frequent recalibrations, thereby increasing operational costs and resource consumption. Cost efficient ion sensors with screen-printed electrodes measuring ion concentrations are demanded, particularly in sectors like agriculture, water monitoring, and industrial processes but may be limited in measurement accuracy due to sensor drift and variation in sensor calibration. To address these challenges posed by sensor drift, the application of machine learning (ML) based algorithms at the device level presents a promising approach. By leveraging ML techniques, it is possible to enhance the accuracy of ion sensors and compensate for drift leading to more reliable monitoring systems. In this paper, results of ML-based drift compensation are presented for the use case of ion sensors to demonstrate the potential benefits. Dedicated experiments were conducted to characterize the concentration sensitivity and drift response of ion sensors, providing essential data for algorithm development. Algorithms were developed for calibration and drift compensation, utilizing regression and Kalman filter techniques, which provide real-time adjustments, thus improving the accuracy of sensor readings.

What this Whitepaper provides:

- Overview of the technology of printed potentiometric ion sensors.
- ML based approaches to address the calibration and drift compensation required for the application:
  - description of experiments to characterize the concentration response and drift behavior of the sensors,
  - algorithms for calibration and drift characterization,
  - realization of a Kalman filter-based approach for real-time drift compensation.
- Environmental impact assessment of the AI system (training and operation).
- Discussion of the results and prospects for further development.

2. Introduction

Ion sensors have become increasingly essential in various industries due to their ability to monitor specific ion concentrations in real-time. Specifically, printed ion sensors are of high interest due to cost efficient manufacturing. Figure 1 shows the printed ion sensor developed at the Fraunhofer IISB.

Reviews of printed ion sensor technology and their application areas can be found in [1–4]. Important sectors of application of ion sensors include

- agriculture, where ion sensors are used to monitor nutrient levels (e.g., nitrate and potassium) in soil and irrigation water, which helps to optimize fertilization and to improve crop yield,
- water quality monitoring, where ion sensors are applied for detecting harmful ions (e.g., heavy metals, nitrates) in drinking water and wastewater treatment, ensuring compliance with health regulations, and
- process monitoring in industry, where ion sensors are applied in various manufacturing processes (e.g., chemical production and food processing) to monitor pH levels and ionic concentrations for quality control.

Figure 1: Printed ion sensor developed at the Fraunhofer IISB (picture: Fraunhofer IISB).

Despite their benefits, several challenges hinder the widespread use of ion sensors:

- Sensor drift: Ion sensors often exhibit drift over time, leading to inaccurate measurements and the need for frequent calibration.
- Temperature sensitivity: Many ion sensors are sensitive to temperature changes, which can affect their accuracy and reliability.
- Interference from other ions: The presence of other ions can interfere with the sensor readings, particularly in complex matrices such as soil or wastewater.
- Limited selectivity: Some ion sensors may not be selective enough for specific ions, resulting in cross-sensitivity and erroneous data.

Several approaches are being explored to address the challenges associated with ion sensors. Calibration algorithms and the application of ML techniques can help to improve accuracy by identifying patterns and compensating for drift and interference. Developing integrated temperature compensation mechanisms can help mitigate the effects of temperature variations on sensor performance. Selective membranes may enhance sensor selectivity and ion-selective electrodes can reduce interference from other ions.

3. Theoretical Background and Approach

Figure 2 shows the working principle of the printed ion sensor manufactured at the Fraunhofer IISB. The printed ion sensor comprises four working electrodes made of silver (Ag) or carbon © and one reference electrode made of silver/silver chloride (Ag/AgCl). The electrodes are encapsulated with a polymer-based material and are manufactured using a screen-printing process. The ion selective working electrode is created by pipetting an ionophore within a polymer matrix onto a suitable electrode (e.g. a graphite electrode), allowing it to selectively interact with specific ions. The reference electrode is designed with a defined polymer matrix that stabilizes its electrochemical potential. To characterize the concentration of ions such as sodium (Na^+), potassium (K^+), and chloride (Cl^-), an electromotive force (*EMF)* is measured between the working electrode and a reference electrode. For initial sensor characterization, the *EMF* is assessed between each sensor electrode and a silver/silver chloride (Ag/AgCl) glass reference electrode. This measurement enables the determination of ion concentrations based on the generated *EMF* values.

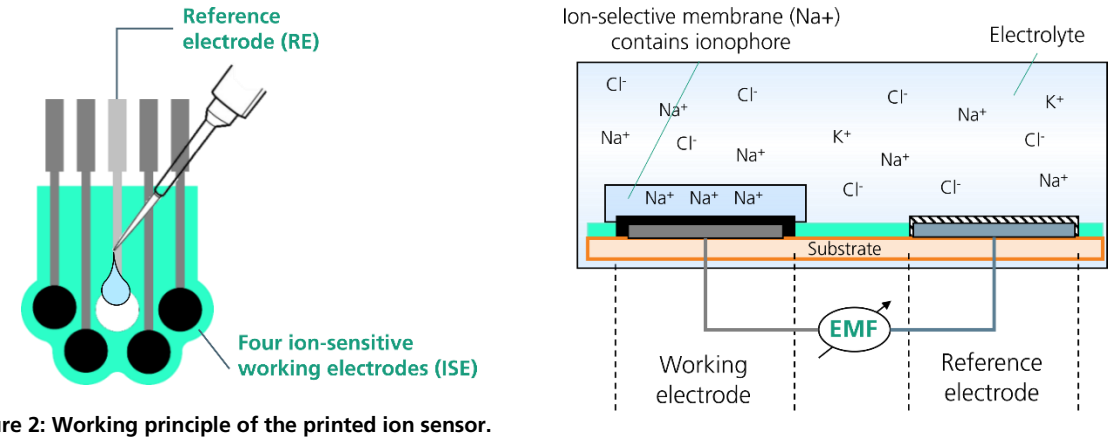

Figure 2: Working principle of the printed ion sensor.

The *EMF* is given by the Nernst equation as:

$$EMF = E^0 + \frac{RT}{Fz_i}\ln(a_i) = E^0 + \ln(10)\cdot\frac{RT}{Fz_i}\log(a_i) \approx E^0 + 2{,}303\frac{RT}{Fz_i}(-\mathrm{pC}),\ \text{with}$$

$$\ln(10) \approx 2{,}303 \text{ and } \mathrm{pC} = -\log(a_i).$$

Here, E^0 is the standard electrode potential, R is the ideal gas constant, T is the absolute temperature, F is Faraday's constant, and z_i is the number of electrons transferred in the cell reaction for ion i. The activity a_i reflects the concentration of the ion i in the solution. The pC value describes the change of concentration of an order of magnitude and is linearly proportional to the measured *EMF*. For a temperature of 298.15 K (25 °C), the sensitivity, i.e., the change in *EMF* per decade of concentration change (pC) is approximately 59 mV. For the printed ion sensors, the exact value for the sensitivity needs to be determined in a calibration process using measurements at different levels of the concentration change in pC vs. the reference glass electrode. The sensitivity may differ between the ion sensitive sensors and the *EMF* value measured with the sensors reference electrode may also not be constant for different concentrations. Moreover, the sensors exhibit an *EMF* drift when measuring over a longer period. In this work, regression and Kalman filter techniques were developed to compensate for these effects to improve the accuracy of the sensor measurements. The approach is described in detail in the next sections.

4. Drift Compensation for the Printed Ion Sensors

4.1 Experimental Characterization of Ion Sensor Drift

Experiments were conducted, which simulate a realistic scenario of fertilizing a field using a drip irrigation system, with a concentration range defined between 1-10 mmol/l. To improve feasibility, the experimental design incorporates a 30-minute fertilization phase followed by a 30-minute dilution phase, with 30-minute constant concentration segments in between each phase. In real-world applications, the holding and decreasing of concentration would occur over even significantly longer duration, typically spanning several hours. Figure 3 shows the experimental setup to provide defined NaCl concentrations vs. time (a) and the shapes of the provided concentration in mmol/ and -pC units are shown in Figure 3 (b – d).

A syringe pump was utilized to dispense a solution with a precisely defined concentration of NaCl at a set flow rate. A magnetic stirrer is employed to ensure rapid distribution of the solution throughout the system. The duration of the solution addition can be programmed to automatically achieve a predetermined target concentration. During the experiment, the concentration between the points $\mathrm{pC} = 3$ (0.1 mmol/l) and $\mathrm{pC} = 2$ (1 mmol/l) is varied, using a higher concentration solution of 100 mmol/l NaCl and a lower concentration solution of distilled water. Each sensor comprised two Na^+ sensitive electrodes and one reference electrode. The sensors were characterized vs. an Ag/AgCl glass reference electrode, and the *EMF* was recorded with a sampling interval of two seconds. Overall, three sensors were investigated.

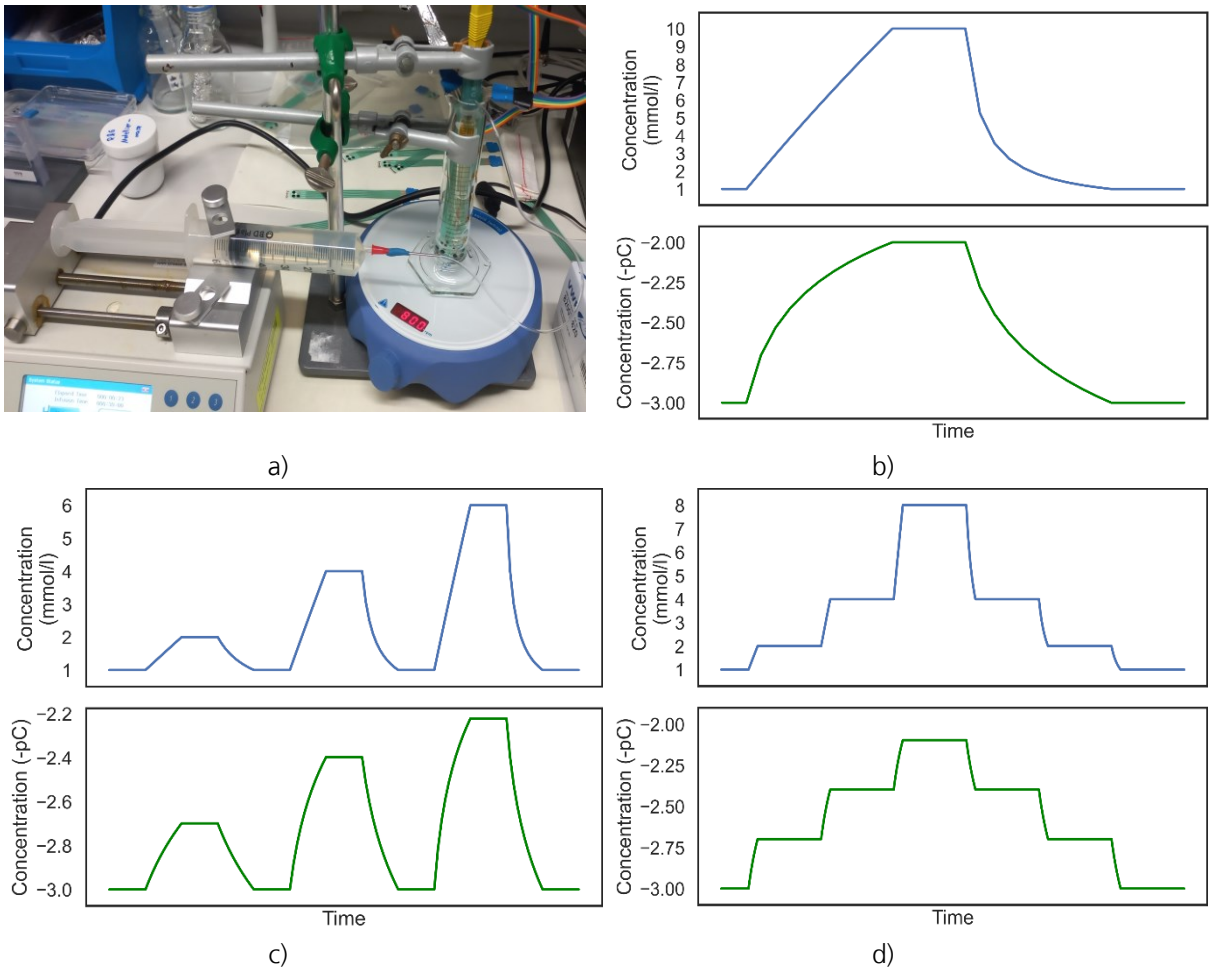

Figure 3: Experimental setup to provide defined NaCl concentrations vs. time (a) and the shapes of the provided concentration in mmol/ and -pC units (b–d) (picture: Fraunhofer IISB).

4.2 Data preparation

Data analysis was conducted in Python and supporting libraries. The recorded *EMF* data measured vs. the Ag/AgCl glass reference electrode were converted to *EMF* values measured between the ion sensitive electrodes of the sensor $EMF_{\mathrm{Na+,\,Re}}$ as:

$$EMF_{\mathrm{Na+,\,Re}} = EMF_{\mathrm{Na+,\,Ag/AgCl}} - EMF_{\mathrm{Re,\,Ag/AgCl}},$$

where $EMF_{\mathrm{Na+,\,Ag/AgCl}}$ and $EMF_{\mathrm{Re,\,Ag/AgCl}}$ are the *EMF* values of the ion sensitive electrode and the reference electrode measured vs. the Ag/AgCl glass reference electrode. Figure 4 (a), (c) show the raw *EMF* values for experiment 1 and experiment 3, respectively. By calculation of the *EMF* vs. the reference electrode, correlated trends and noise in the measurement vs. the Ag/AgCl glass reference electrode are compensated. Still, the *EMF* indicates a linear drift vs. time and different initial points of the *EMF*.

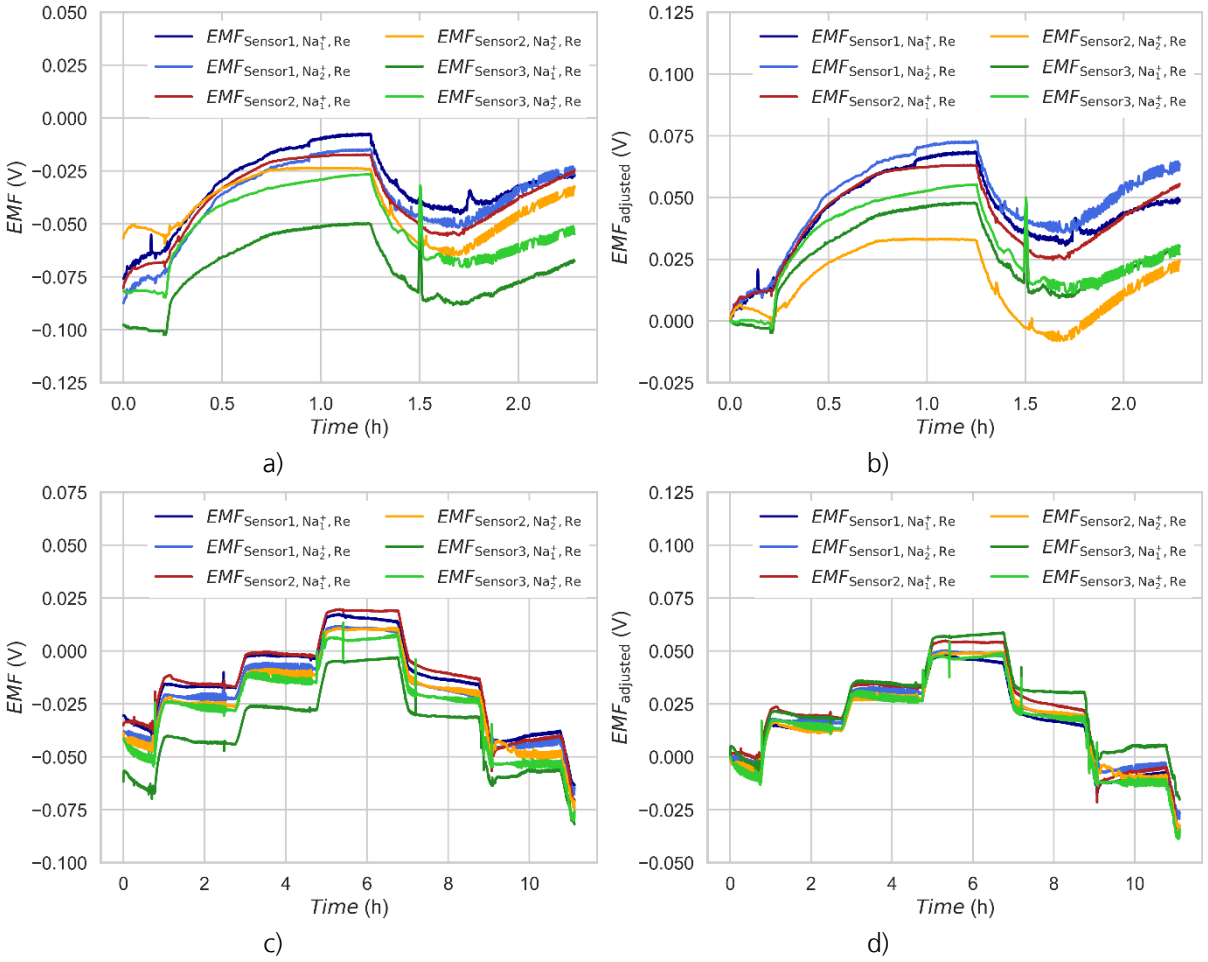

Figure 4: Raw EMF values for experiment 1 and experiment 3 (a), (c) and traces with adjusted offset to *EMF* = 0 at *t* = 0 (b), (d).

To compensate for the offset in the initial points (Figure 4 (a), (c)), the offset was adjusted to 0 V, i.e., the change in *EMF* is normalized to the *EMF* value at the initial concentration value (Figure 4 (b), (d)). The sensor traces show similar trends but in detail still differ in their *EMF* values. Experiment 2, not shown for reasons of space, showed similar trends but also less reproducibility in the regions where the solution was diluted, as this was achieved by addition of distilled water and, if necessary, removing excess solution.

4.3 Calibration and Drift Compensation

As seen in Figure 4 (b), (d)., the sensors will not match the theoretical sensitivity values of 59 mV as expected from theory when changing concentration from 1 to 10 mmol/l and moreover the sensitivity is different for each selective electrode. Additionally, the traces show drifts and hence, the *EMF* values will not return to the same values, whenever the concentration is reduced to the initial values. As an initial calibration of the sensors was not available, the sensors were calibrated using the sensors trace data. The calibration of the measured *EMF* traces to the theoretically expected *EMF* values was conducted by linear regression assuming that the *EMF* traces are overlaid by a linear drift:

$$EMF_{\mathrm{N}} = EMF_{\mathrm{N},\,c} + \varepsilon = a \cdot EMF_{\mathrm{adjusted}} + b \cdot t + \varepsilon = EMF_{\mathrm{adjusted,\,cal.}} + EMF_{\mathrm{d,\,linear}} + \varepsilon,$$

where EMF_{N} is the reference *EMF* as expected from the Nernst equation due to the introduced concentration changes, $EMF_{\mathrm{N},\,c}$ reflects the corresponding measured concentration response, EMF_{adjusted} is the *EMF* adjusted to 0 V at $t = 0$, t is time, a, b are model coefficients and ε is the remaining error. Hence, the sensor traces can be separated into a calibrated *EMF* component $EMF_{\mathrm{adjusted,\,cal.}}$ and a drift component $EMF_{\mathrm{d,\,linear}}$. Figure 5 shows the separation of the different trace components.

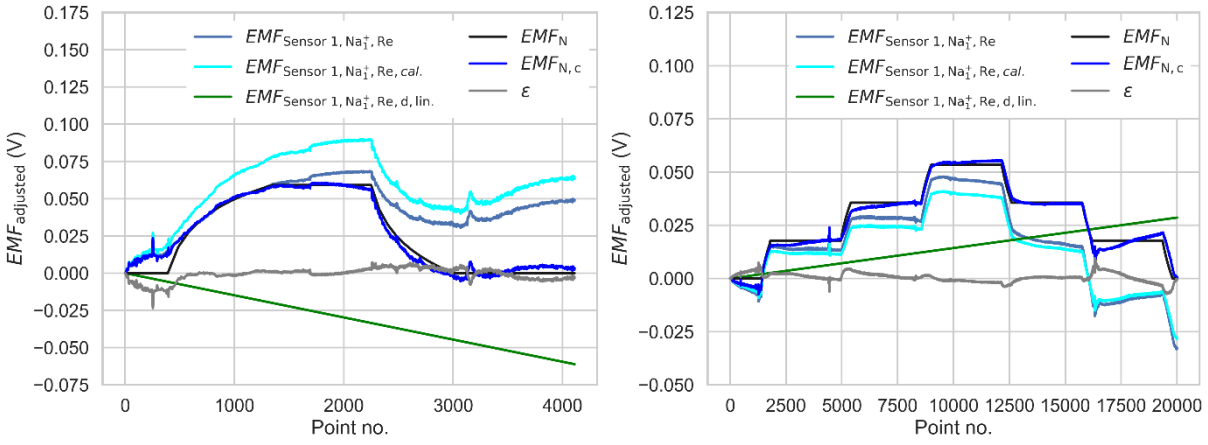

Figure 5: Separation of the trace components to match the *EMF* values by the concentration changes to the values as expected from the Nernst equation for the Na^+ sensitive electrode 1 of sensor 1 (experiment 1 (a), experiment 3 (c)).

The average and range values of the coefficients, which were determined for the different experiments, sensors, and electrodes are summarized in Table 1. Typically, the coefficient *a* shows larger ranges for the sensors indicating their difference in the sensitivity, when uncalibrated. The coefficient *b* for experiment 1 differs from those in experiment 2 and 3, which show more consistent values. The differences may be induced by differences in the experiments due to inhomogeneous solution mixture in the small cells and disturbances when diluting the solution and removing excess solution.

Table 1: Average and range values of the coefficients, which were determined for the different experiments, sensors, and electrodes.

Experiment	Coefficient	Average	Range
1	a	1.43	0.48
	b	-0.0104 mV/point	0.0157 mV/point
2	a	0.69	0.29
	b	0.0010 mV/point	0.0023 mV/point
3	a	0.81	0.11
	b	0.0013 mV/point	0.0007 mV/point

A Kalman filter was implemented to compensate the sensor drift assuming that the sensors are calibrated and the drift rate for each sensor can be characterized by a linear trend as given in in Table 1 and drift rate for each sensor can be derived as mean value over the sensors. The Kalman filter assumes an evolvement of the state described by the model:

$$\mathbf{EMF}_k = \mathbf{F} \cdot \mathbf{EMF}_{k-1} + \mathbf{B} \cdot \boldsymbol{u}_{\boldsymbol{k-1}} + \mathbf{w}_{\boldsymbol{k-1}},$$

Where $\mathbf{F}$ is the state transition matrix is applied to the previous state of the variable, $\mathbf{B}$ is the control-input matrix, which is applied to the control vector $\mathbf{B}$, and $\mathbf{w}$ is the process noise, which is assumed to be drawn from a zero mean multivariate normal distribution. To estimate the different components, i.e., the calibrated $EMF_{\mathrm{adjusted,\,cal.}}$, the drift component $EMF_{\mathrm{d,\,linear}}$, which sum up to the expected concentration value of the true concentration $EMF_{\mathrm{N},\,c}$, the components for the calculation per data point k are arranged as:

$$\begin{bmatrix} EMK_{\mathrm{m,\,adjusted,\,cal.},\,k} \\ EMF_{\mathrm{N,\,c},\,k} \\ EMF_{\mathrm{d,\,linear},\,k} \end{bmatrix} = \begin{bmatrix} 1 & 0 & 0 \\ 1 & 0 & 1 \\ 0 & 0 & 1 \end{bmatrix} \cdot \begin{bmatrix} EMK_{\mathrm{m,\,adjusted,\,cal.},\,k-1} \\ EMF_{\mathrm{N,\,c},\,k-1} \\ EMF_{\mathrm{d,\,linear},\,k-1} \end{bmatrix} + \begin{bmatrix} 0 & 0 & 0 \\ 0 & 0 & 0 \\ 0 & 0 & b \end{bmatrix} \cdot \begin{bmatrix} 0 \\ 0 \\ 1 \end{bmatrix} + \mathbf{w}_{\boldsymbol{k}},$$

where the drift is modeled by its previous value and the coefficient b in the control matrix. At time step k a measurement $\mathbf{z}_k$ of the true state $\mathbf{EMF}_k$ is conducted to:

$$\mathbf{z}_k = \mathbf{H} \cdot \mathbf{EMF}_k + \mathbf{v}_k,$$

where $\mathbf{H}$ is the measurement matrix and $\mathbf{v}_k$ is the measurement noise, which is assumed to be zero mean Gaussian white noise with covariance $\mathbf{R}_k EMF_{\text{adjusted, cal.}}$ can be measured, the measurement matrix is given as:

$$\mathbf{H} = [1 \quad 0 \quad 0].$$

Figure 6 shows the predictions for experiment 1 and 3, where the example is given for sensor 1 and electrode 1. Figure 6 (a) and (c) show the predictions and true values of the adjusted *EMF* for calibrated sensor ($EMF_{\text{adjusted, cal.}}$), the drift component ($EMF_{\text{d, linear}}$), and the *EMF* value due to the concentration change ($EMF_{\text{N, }c}$) if the coefficient b was exactly known, e.g., from the calibration process. Here, the adjusted *EMF* ($EMF_{\text{adjusted, cal.}}$), and drift component ($EMF_{\text{d, linear}}$) are precisely predicted and the *EMF* value due to the concentration change ($EMF_{\text{N, }c}$) is also well reflected. If the average value of b is used in the predictions (Figure 6 (b), (d)) for the adjusted *EMF* ($EMF_{\text{adjusted, cal.}}$) are also precise but the predictions for the drift component and the *EMF* value due to the concentration change ($EMF_{\text{d, linear}}$, $EMF_{\text{N, }c}$) will depend on the deviation of the average of coefficient b from the precise value obtained for the sensor. Overall, if the sensors are calibrated and characterized by their drift behavior, Kalman filtering provides an efficient method for real-time drift compensation.

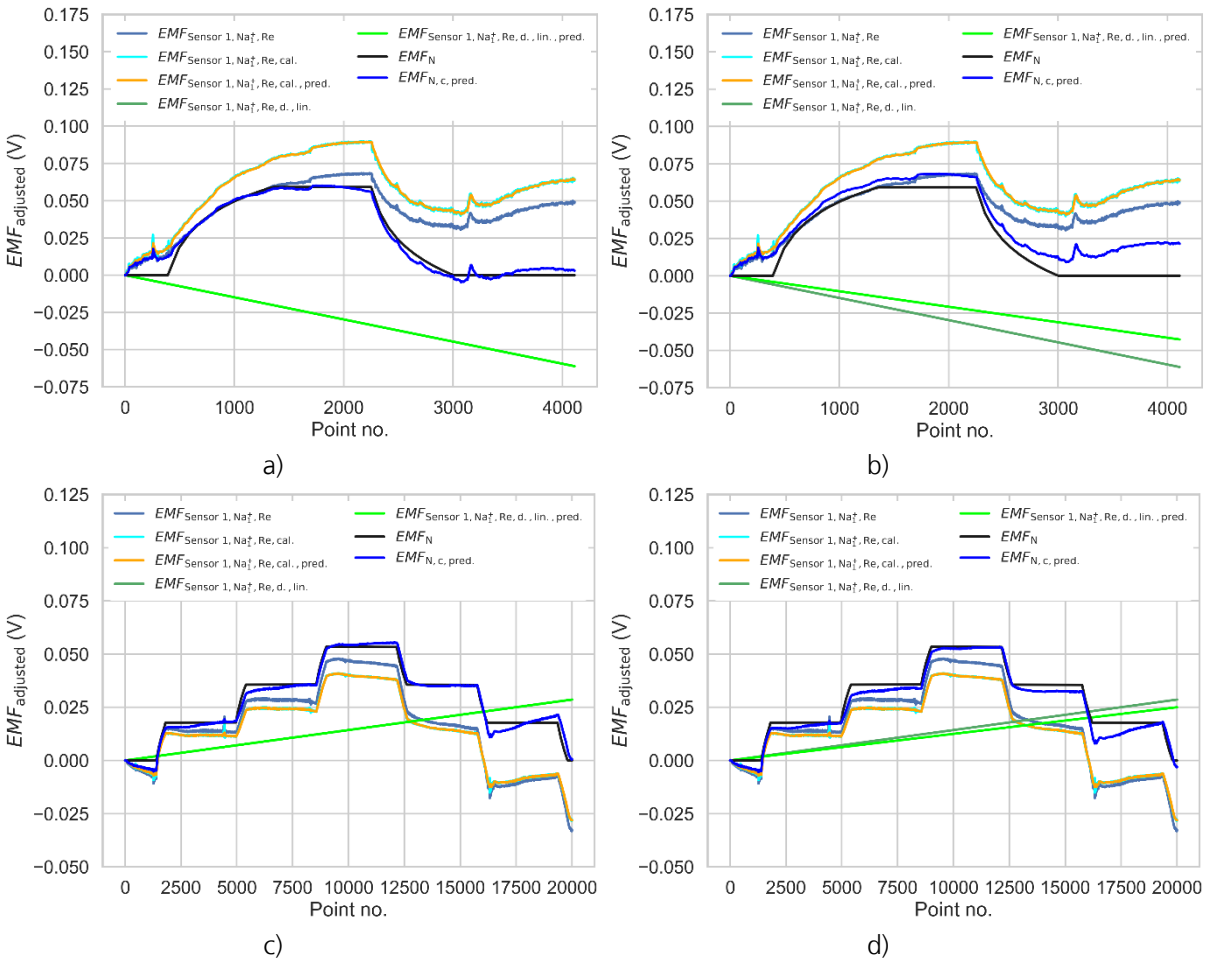

Figure 6: Predictions of the $EMF_{\text{adjusted, cal.}}$, the drift component $EMF_{\text{d, linear}}$, and the true concentration value $EMF_{\text{N, }c}$ for experiment 1 and 3, where the example is given for sensor 1 and electrode 1. The predictions are given for the case that the drift coefficient is known (a), (c) or is derived from an average over several measurements (b), (d).

4.3 Environmental Impact Assessment of the AI System

For the environmental impact assessment, a concept was developed that comprises two components:

- Definition of the system architecture of the sensor system with integrated drift compensation.
- Life cycle assessment of the AI system (training and operation).

Figure 7 shows the architecture of the sensor system, consisting of the ion sensor with associated measurement electronics, as well as the AI system for calibration and drift compensation. This architecture forms the basis for the following life cycle assessment.

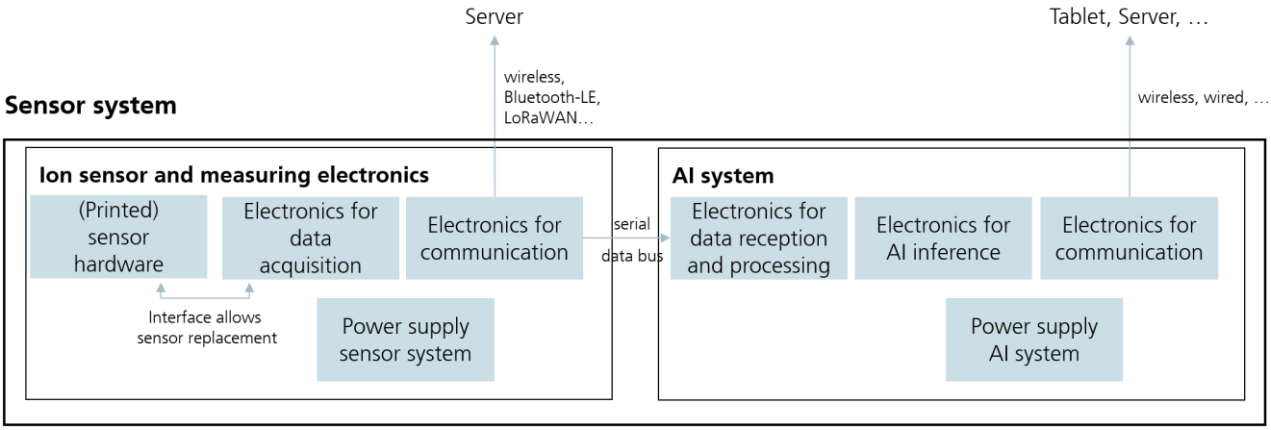

Figure 7: System architecture of the sensor system with integrated drift compensation.

For the assessment of the AI system, two approaches to implementing the algorithms for calibration and drift compensation were compared: the use of filter-based methods (e.g., Kalman filters) and the use of neural networks. For both approaches, the factors of computational complexity, training duration, runtime, and hardware requirements were considered, and the respective total energy requirements were estimated. The results are summarized in Table 2 and support the approach pursued in the project of relying on filter-based methods: The estimated energy requirement of less than 1 kWh over 10 years when using filter-based methods contrasts with just under 50 kWh when using a neural network.

Table 2: Assessment of the AI system.

Factor	Filter-based methods	Neural Networks
Computational complexity	Moderate (linear algebra operations)	High (depending on architecture)
Training duration (see below)	Short to moderate	Long (depending on architecture)
Runtime	Shorter than neural networks	Medium (for this application)
Hardware requirements	Powerful CPU (if necessary: GPU)	Specialized hardware (GPU, TPU)
Total energy consumption	low 10 years: 810 Wh	moderate 10 years: 49 kWh
Training:	1x 2h * 100 W = 200 Wh One-time 200 Wh	3x/year * 5 h * 300 W 4,5 kWh per year
Runtime / inference: (Raspi 4: max. 15 W)	24x/day * 5 sec * 5 W 61 Wh per year	24x/Tag * 10 sec * 15 W 365 Wh per year

5. Discussion

Drift compensation and calibration of ion sensors are critical for ensuring accurate measurements in various sensor applications, e.g., for the investigated printed ion sensors. In the literature, several techniques were developed and presented to detect and compensate for drift, which can be distinguished in the main approaches as summarized in Table 3, each with specific algorithmic solutions [5]. Among the various techniques employed, Kalman filtering has emerged as a prominent solution due to its ability to estimate the state of a dynamic system from noisy observations, e.g., by capturing the sensor dynamics and compensating for drift by continuously updating the state estimates based on new measurements. ML techniques have gained traction in recent years for drift compensation in ion sensors. Approaches such as neural networks, support vector machines, and regression techniques have been employed to model sensor behavior and predict drift. This adaptability can be particularly beneficial in environments where sensor characteristics may evolve over time. However, ML methods often require large datasets for training and can be susceptible to overfitting, especially when the data is limited. Furthermore, the interpretability of ML models can be a challenge, which is crucial for applications requiring clear insights into sensor behavior. In contrast, Kalman filtering provides a more interpretable and leaner framework for understanding the sensor dynamics and drift compensation. In addition, the environmental impact assessment showed the benefit of this approach regarding total energy consumption.

Table 3: Main approaches to detect and compensate for sensor drift.

Approach	Advantage	Disadvantage
Manual recalibration of sensors at regular intervals	Simple	• Time-consuming • Not applicable for many sensors
Automated calibration using fitted parametric models, e.g., polynomial curves or signal-processing approaches	Adaptation to characterizable trends	• Not applicable to changing behavior, nonlinear and unknown influences without refitting • Ground truth samples required
Kalman filtering and other recursive estimation techniques	Efficient calculation for modeling drift in real time	• Predefined accurate model of the drift process required
ML learning and deep learning	ML can learn drift characteristics from data	• Computationally intensive • Higher environmental impact • Large amount of data required

The approaches for developing calibration and drift compensation algorithms presented here, base on the balancing of practical constraints. The initial strategy prioritizes minimal data requirements for sensor characterization and ML algorithm development, with inference designed to be computationally efficient on edge devices. As larger datasets become available, e.g., after volume production, if needed, more advanced ML techniques for drift compensation may be adopted. The algorithm and drift-compensation design align with current trends in manufacturing reproducible potentiometric sensors, as reported in [6], specifically addressing inter-sensor reproducibility of E^0 and concurrent drift mechanisms such as those induced by water immersion. Enhancing sensor reproducibility is expected to enable more consistent characterization of sensor properties and more robust drift models; our current studies already show comparable values. This approach provides a strong foundation and flexible path for parallel sensor optimization and extended characterization, including the dynamics under concentration changes or dilution due to water exposure, as well as evaluation under real-world operating conditions.

6. Conclusion and Outlook

This work demonstrates that lightweight, device-level ML—combining regression with Kalman filtering—can effectively compensate for the drift in cost-efficient ion sensors with screen-printed electrodes. Dedicated experiments quantified concentration sensitivity and drift behavior, enabling calibration and real-time drift correction on edge hardware. The approach improves accuracy, addresses optimized calibration and reduced recalibration frequency, and supports further development towards reliable, low-cost and low-energy monitoring across agriculture, water quality, and industrial processes. These results indicate a viable pathway to scalable, data-driven sensor operation without heavy computational or data demands. Looking ahead, ongoing efforts to stabilize sensor materials, manufacturing reproducibility, and packaging are expected to reduce drift and inter-sensor variability, further simplifying and strengthening the applicability of on-device ML models. As larger datasets become available from pilots and volume deployments, drift-compensation may be addressed for a broader data base and for improved transferability across sensor batches.

Overall, our work successfully demonstrates the feasibility of lightweight, edge-deployable ML, which can compensate for drift in low-cost ion sensors and bridges the gap from lab characterization application to robust field performance for the transition to stable, scalable and environmentally friendly sensor ecosystems.

7. Acknowledgment

The work presented is part of the »Green ICT @ FMD« project. The project is established by the Research Fab Microelectronics Germany and funded by the German Federal Ministry of Research, Technology and Space.

References

[1] G. Polidori, S. Tonello, and M. Serpelloni, "Ion-Selective All-Solid-State Printed Sensors: A Systematic Review," *IEEE Sensors J.*, vol. 24, no. 6, pp. 7375–7394, 2024, doi: 10.1109/JSEN.2024.3354321.

[2] P. Goodrich *et al.,* "Fully-Printed Ion Sensor Arrays for Measuring Agricultural Nitrogen and Potassium Concentrations Using Nernstian and AI Models," *Advanced Sensor Research*, vol. 4, no. 4, 2025, Art. no. 2400121, doi: 10.1002/adsr.202400121.

[3] D. Song, C. Mao, C. Jiang, R. Liang, and G. Lisak, "Printed potentiometric sensors," *TrAC Trends in Analytical Chemistry*, vol. 192, p. 118420, 2025, doi: 10.1016/j.trac.2025.118420.

[4] A. M. Al-Amri, "Printed Sensors for Environmental Monitoring: Advancements, Challenges, and Future Directions," *Chemosensors*, vol. 13, no. 8, p. 285, 2025, doi: 10.3390/chemosensors13080285.

[5] A. Krayden, M. Avraham, H. Ashkar, T. Blank, S. Stolyarova, and Y. Nemirovsky, "TinyML-Based Real-Time Drift Compensation for Gas Sensors Using Spectral–Temporal Neural Networks," *Chemosensors*, vol. 13, no. 7, p. 223, 2025, doi: 10.3390/chemosensors13070223.

[6] Y. H. Cheong, L. Ge, and G. Lisak, "Highly reproducible solid contact ion selective electrodes: Emerging opportunities for potentiometry - A review," *Analytica chimica acta*, early access. doi: 10.1016/j.aca.2021.338304.